Dislocation Density Tensor Characterization of Deformation Using 3D X-Ray Microscopy

B. C. Larson[1]
e-mail: bcl@ornl.gov

J. Z. Tischler

Materials Science and Technology Division,
Oak Ridge National Laboratory,
Oak Ridge, TN 37831

Anter El-Azab[2]
Mechanical Engineering Department,
Florida State University,
Tallahassee, FL 32310

Wenjun Liu
Advanced Photon Source,
Argonne National Laboratory,
Argonne, IL 60439

Three-dimensional (3D) X-ray microscopy with submicron resolution has been used to make spatially resolved measurements of lattice curvature and elastic strain over two-dimensional slices in thin deformed Si plates. The techniques and capabilities associated with white-beam 3D X-ray microscopy are discussed, and both theoretical and experimental considerations associated with the measurement of Nye dislocation density tensors in deformed materials are presented. The ability to determine the local geometrically necessary dislocation (GND) density in the form of a dislocation density tensor, with micron spatial resolution over mesoscopic length scales, is demonstrated. Results are shown for the special case of an elastically bent (dislocation free) thin Si plate and for a similar thin Si plate that was bent plastically, above the brittle-to-ductile transition temperature, to introduce dislocations. Within the uncertainties of the measurements, the known result that GND density is zero for elastic bending is obtained, and well-defined GND distributions are observed in the plastically deformed Si plate. The direct and absolute connection between experimental measurements of GND density and multiscale modeling and computer simulations of deformation microstructures is discussed to highlight the importance of submicron-resolution 3D X-ray microscopy for mesoscale characterization of material defects and to achieve a fundamental understanding of deformation in ductile materials. [DOI: 10.1115/1.2884336]

1 Introduction

Lattice defects in crystalline materials, such as point defects, defect clusters, dislocations, grain boundaries, and inclusions, play an important role in determining the strength of materials. Indeed, processing of materials often aims to adjust the types and density of such defects to achieve certain strength and performance objectives. For example, the processing of metallic materials, especially structural alloys, uses multiple thermomechanical steps to adjust the phase composition, texture, and grain size distribution in the alloy. For the class of structural alloys, however, plastic deformation, which is dominated by a collective dislocation behavior, is a central issue of mechanical behavior. For this reason, the study of dislocations and their behavior in the context of metal deformation has been at the core of the mechanical metallurgy field; the conceptual, theoretical, and experimental accomplishments dating back to the 1950s when dislocations were first observed in the electron microscope now constitute the well known theory of dislocations [1,2].

Transmission electron microscopy (TEM) provides very high spatial resolution and is unequalled for imaging individual dislocations and related defects. X-ray microscopy and electron microscopy represent complementary tools for the investigation of deformation-induced defects in crystals. Although X-rays are able to image single dislocations in highly perfect crystals [3], the dislocation density in deformed crystals quickly becomes too high for single dislocation imaging to be feasible using X-rays. On the other hand, X-rays are able to provide crystal deformation information on much larger length scales [4–7]. For instance, the collective nature of dislocation aggregation and patterning over mesoscopic length scales (tenths of microns to hundreds of microns) cannot be addressed effectively by TEM. Moreover, the penetration power of X-rays makes it possible to probe elastic strain and lattice curvature induced by dislocation distributions nondestructively (i.e., without sectioning the samples for observation) [5,7,8]. Furthermore, on mesoscopic length scales, the response of dislocation density, rather than individual dislocations, to both applied and self-generated stresses becomes critical in understanding their overall evolution.

As discussed in recent reviews [9–12] and as is evident from the increasing activity associated with spatially resolved 3D X-ray investigations of materials [13], we are in the midst of a revolution in spatially resolved X-ray investigations of materials. This revolution is driven scientifically by the fact that critical properties of almost all materials of significant technological and scientific interest derive from the heterogeneity of the material microstructure and its complex and hierarchical nature. Revolutionary advances in X-ray microscopy capabilities have been fueled by rapid developments in X-ray optics, high brilliance synchrotron X-ray sources, and high-resolution charge coupled device (CCD) X-ray area detectors, and by the development of new and powerful 3D X-ray microscopy techniques.

Two types of three-dimensional diffraction x-ray microscopy have been developed [9]. One in the form of "3D crystal microscopy" [11,14,15], as developed by RISØ at the ESRF, utilizes high-energy monochromatic X-rays in the range of ~50 keV; it is a powerful technique that has been widely applied for the investigation of deformation in materials as well as other applications. This technique uses a rotating crystal method and has demonstrated spatial resolution down to a few microns [11]. The second technique (the one used in this study) is medium energy (5–25 keV) white-beam 3D X-ray microscopy as developed by Oak Ridge National Laboratory (ORNL) at the Advanced Photon Source (APS) facility [4–10,13,16]. It achieves point-to-point submicron spatial resolution through the use of differential-aperture (knife-edge) depth profiling.

In this paper, we review the differential-aperture X-ray microscopy (DAXM) method for achieving submicron spatial resolution

[1]Corresponding author.
[2]Also at School of Computational Science, Florida State University, Tallahassee FL 32306.

Contributed by the Materials Division of ASME for publication in the Journal of Engineering Materials and Technology. Manuscript received September 20, 2007; final manuscript received January 4, 2008; published online April 2, 2008. Assoc. Editor: Matthew P. Miller. Paper presented at the Materials Processing Defects 5, 2007.

Copyright © 2008 by ASME

Downloaded 04 Sep 2009 to 160.91.157.167. Redistribution subject to ASME license or copyright; see http://www.asme.org/terms/Terms_Use.cfm

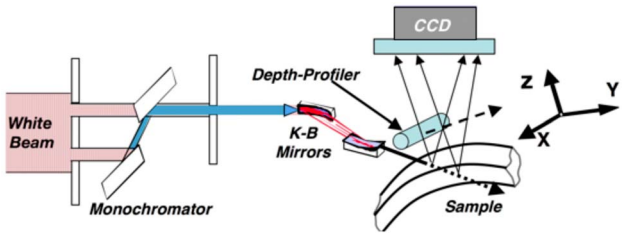

Fig. 1 Schematic view of the beamline configuration for the XOR/UNI Sector 34 3D X-ray microscopy facility at the APS. White synchrotron radiation is incident onto upper and lower slits that pass either white radiation directly to the crossed K-B mirrors (top) or, reflecting off the two-bounce monochromator (bottom), deliver a scanning monochromatic beam to the mirrors. The beam is focused to ~0.5 μm at the position of the schematic bent-plate sample. A CCD area X-ray detector is mounted at 90 deg to the incident microbeam, and the depth-profiler wire is advanced with submicron steps through the diffracted beams to obtain 3D spatial resolution.

in three dimensions [4] and demonstrate the use of 3D X-ray microscopy to measure the geometrically necessary dislocation (GND) density over mesocopic length scales in elastically and plastically deformed thin silicon plates. The dislocation density tensor as introduced by Nye more than 50 years ago [17] is an important and fundamental quantity characterizing dislocation distributions in crystals, and it serves as a direct link between experimental measurements and computational modeling of deformation [18–21]. This paper extends results demonstrated for 3D measurements of dislocation density tensors with micron spatial resolution along a single line in elastically and plastically deformed Si plates [5] to measurements over an areal slice within deformed Si plates. The results represent the first demonstration of nondestructive, point-to-point, micron-resolution 3D X-ray microscopy determinations of full dislocation density tensors over a mesoscopic area in bulk material. The theoretical background associated with dislocations in elastic media is discussed in relation to elastic strain and lattice rotations in deformed crystals as measured by the X-ray technique described here. The importance of nondestructive, spatially resolved measurements of local lattice strain and lattice rotation is emphasized, and the connection between these measurements and emerging mesoscale models of deformation based on dislocation density evolution is discussed.

2 Submicron-Resolution 3D X-Ray Microscopy

As mentioned above, the confluence in the last 10–15 years of high brilliance synchrotron X-ray sources, high precision X-ray focusing optics, and high-performance CCD X-ray detectors has led to revolutionary advances in spatially resolved X-ray probes [9]. Although the DAXM (knife-edge profiling) experimental technique has been described previously, important aspects of the differential-aperture approach to depth profiling and 3D X-ray microscopy will be recalled here for completeness.

Figure 1 shows a schematic illustration of the DAXM technique in which either white (polychromatic) or monochromatic synchrotron X-rays are directed to crossed Kirkpatric–Baez focusing mirrors. The achromatic nature of forward scattering mirrors focuses all wavelengths to the same point with an ~0.5 μm diameter and an ~0.5–1 mm depth of field. White microbeams produce full Laue diffraction patterns from each part of the sample irradiated by the microbeam, so rotations of the sample are not used during measurements [16]. The use of submicron X-ray beams provides a two-dimensional (2D) spatial resolution perpendicular to the beam direction; however, the diffraction patterns from each submicron length segment along the beam are superposed on the CCD detector and must be resolved.

The DAXM technique depth resolves entire Laue diffraction patterns from each micron (or submicron) segment along polychromatic microbeams. Depth-resolved information is extracted by collecting diffraction patterns on the CCD detector for each step of the profiler wire (50 μm Pt in this case) as the wire is translated through the Laue diffraction patterns [4,6,22]. The distance from the profiler to the sample surface is normally less than 200 μm, while the distance from the profiler to the detector is usually in the range of 30–50 mm; therefore, the 24 μm pixel size of the CCD contributes only ~0.1 μm of parallax at the microbeam position. Of course, a micron width aperture would be preferred for performing depth sorting, but for the hard X-rays (5–25 keV) used here would require slits with ~10 μm thickness. This would be more of a collimator passing only a few degrees of the angular spread of the diffraction pattern, whereas the full (>45 deg) angular range of the Laue diffraction pattern striking the detector is required. The circular cross section of the Pt wire ensures that diffracted rays at all angles are occluded by the same profiler shape, independent of angle. Therefore, by knowing the position of the wire and the position of a particular pixel, it is possible to triangulate back to the microbeam position to determine the source of diffracted rays on the detector. By successive CCD image collection, submicron wire stepping, image subtraction, and pixel-by-pixel triangulation back to the beam position, computer collation can be used to reconstruct entire (white-beam) Laue diffraction patterns from each segment along the microbeam. The individual depth-resolved diffraction patterns can then be analyzed as diffraction from single points (depths) along the microbeam using the same crystallographic analysis techniques developed for white microbeam diffraction from thin films [16,23].

Since this process produces full diffraction patterns for each depth, it is possible to determine the crystallographic orientation by automated computer indexing of the 10–50 peak Laue diffraction patterns; it is further possible to analyze the details of the diffraction patterns to extract deviatoric (cell shape) elastic strain. Dilatation (lattice expansion/compression) strain information can be obtained using the scanning monochromatic beam capability shown in Fig. 1 [13,23], where monochromatic beams provide energy information to be used in connection with the angular information provided by the CCD detector to obtain absolute lattice parameter measurements using individual Bragg diffracted beams. By performing scans of the Pt wire depth profiler for each position of the microbeam in a 2D area scan over the surface of the sample, local orientations and deviatoric strain tensors can be determined for micron or submicron 3D voxels over mesoscopic volumes within samples. As discussed below, such measurements are significantly more challenging in deformed than in nondeformed materials, and extracting the dilatation component of the elastic strain tensors has, so far, only been automated for special cases [13].

Before discussing the application of 3D X-ray microscopy to deformed materials, we recall briefly an example of measurements of local crystallographic orientations for the nondeformed, polycrystalline case to illustrate the procedure of local orientation determination. Figure 2 shows a color-coded 3D grain orientation mapping of individual grains in nondeformed polycrystalline Al [6,10], where each voxel in the image represents a micron-resolution volume in three dimensions at which the crystallographic orientation was determined. The dark (blue) grain is shown in a position spatially separated from its position in the polycrystal to demonstrate how electronic sorting of voxels by orientation makes it possible to visualize and inspect the morphology of individual grains as well as to view lattice orientations on slices within the volume of the measurement. Nondeformed materials, such as the individual grains in Fig. 2, produce sharp diffraction spots so that an angular resolution of ~0.01 deg can be obtained and strain tensor measurements with $\sim 10^{-4}$ resolution are possible on a submicron resolution point-to-point basis [4,13].

Downloaded 04 Sep 2009 to 160.91.157.167. Redistribution subject to ASME license or copyright; see http://www.asme.org/terms/Terms_Use.cfm

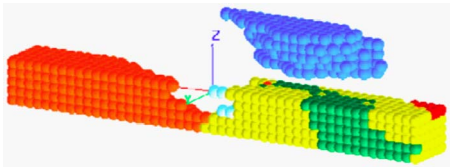

Fig. 2 Color-coded grain structure measured on commercial purity (1% Si,Fe) polycrystalline Al using 3D X-ray microscopy. The individual voxels represent micron spaced points in three dimensions at which local orientations were determined; one of the grains has been separated from its position in the sample to illustrate the use of electronic orientation grouping.

Figure 2 demonstrates the rather well developed application of the 3D X-ray microscopy technique to determine local orientations in a material with little or no intragrain elastic strain or rotational deformation. The thrust of this paper is to demonstrate the status of its use for the determination of GND density distributions in deformed materials, in particular, to determine GND distributions contiguously over a mesocopic length scale area; this entails determining tensor information on lattice curvature and elastic strain gradients at each point.

Although the technique for determining local orientations and local strain tensors in deformed materials is, in principle, the same as that in nondeformed materials, curvature within individual measurement voxels leads to elongated (i.e., streaked) spots rather than sharp, round diffraction spots. This impacts both the resolution and accuracy of orientation and strain tensor measurements [5] because analysis techniques for deconvoluting streaked diffraction patterns within the 3D X-ray microscopy technique are not available at present. For small deformations and elastically stiff materials, the peak smearing is relatively small and can be handled using the centroid of smeared diffraction peaks; both deviatoric strain and local orientations can be obtained with good resolution in such cases [4,6,13].

For deformation in ductile materials, which typically have significantly distorted or streaked Laue spots, measuring strain tensors using white-beam patterns becomes a larger issue. This is because elastic strain is detected by the measurement of relatively small deviations in the angles between individual Laue diffraction spots. Therefore, without deconvolution of the spots, obtaining accurate ($\sim 10^{-4}$) elastic strain tensor information directly from white-beam diffraction patterns in ductile deformed materials is not feasible. On the other hand, local orientations (and, hence, point-to-point misorientations used to determine rotational strain) can be obtained with a few hundredths of a degree angular resolution, even for cases with relatively strong deformation. This is because the local orientation is a function of the collective (average) orientation of all the Laue spots, not deviations between individual spots. Therefore, local orientation measurements can usually be made in ductile deformed samples with a precision of $\sim$0.02 deg; this is somewhat degraded from the $\sim$0.01 deg or better precision capabilities in undeformed materials [4,6,13]. We comment that monochromatic Bragg diffraction techniques have been developed for microbeams that provide absolute lattice parameters with $\sim 10^{-4}$ accuracy from highly streaked [13] as well as relatively sharp diffraction patterns [8]. Unfortunately, monochromatic measurements can be performed on only one reflection at a time, so they are, in general, much more tedious to perform than white-beam measurements. Determinations of full strain tensors with monochromatic techniques would require measurements on at least three noncollinear reciprocal lattice vectors for each voxel and have not been carried out so far. These issues will be revisited in connection with the discussion of the experimental techniques and results in Secs. 4–6 below.

3 Dislocations in Crystalline Materials

The theory of dislocations is a huge subject covering many physical and mechanical characteristics of dislocations in various types of crystals. Here, we focus on the mechanical aspects of dislocations in deformed crystals due to their connection with both the theory of mesoscale deformation and with the theoretical basis of the measurements presented here. Specifically, we discuss the elastic field of dislocations in two cases: the case of a discrete dislocation system containing a large number of dislocations and the case of a continuous distribution of dislocations. Understanding the mechanical effects induced by a system of discrete dislocations is at the heart of the formalism of the dislocation dynamics simulation method [24,25] and the statistical theory of dislocations [26,27]. Continuous dislocation distributions and associated mechanical effects, on the other hand, are the subject of the continuum theory of dislocation fields [28–30]. Models based on these theories are currently used as the basis for understanding plastic deformation of metals at the mesoscale [31]. The connection between synchrotron X-ray microbeam measurements characterizing dislocations in deformed crystals and these theoretical methods is discussed in a recent contribution by the present authors [5].

Like most crystal defects, dislocations have elastic fields [1,32]. For a single dislocation, for example, a closed dislocation loop L with Burgers vector $\mathbf{b}$, this elastic field is described within the linear theory of elasticity by the displacement field,

$$u_m(\mathbf{r}) = -\int_A dA_j b_i c_{ijkl} \frac{\partial}{\partial x_l'} \hat{u}_{mk}(\mathbf{r}' - \mathbf{r}) \tag{1}$$

in which A is an arbitrary open area bounded by the dislocation loop L, c_{ijkl} is the elasticity tensor of the crystal, $\mathbf{r}=(x_1,x_2,x_3)=(x,y,z)$ is the field point, $\mathbf{r}'$ is a point of A, and $\hat{u}_{mk}(\mathbf{r}'-\mathbf{r})$ is the elastic Green's function. The elastic strain can be found from the above displacement field [1],

$$\varepsilon_{ml}(\mathbf{r}) = \frac{1}{8\pi}\oint_L dx_k' b_p \left[\left(-\frac{1}{2}\delta_{km} e_{pql} - \frac{1}{2}\delta_{kl} e_{pqm} + \delta_{lm} e_{pqk} \right) \frac{\partial}{\partial x_q} \nabla^2 R - \frac{1}{1-\nu} e_{pjk} \frac{\partial^3 R}{\partial x_i \partial x_j \partial x_m} \right] \tag{2}$$

This elastic strain field can be used to determine the stress field via Hooke's laws: $\sigma_{ij}=c_{ijkl}\varepsilon_{kl}$. In the above equation, δ_{km} is the Kronecker delta, e_{pql} is the permutation symbol, $R=|\mathbf{r}'-\mathbf{r}|$, and $\mathbf{r}'$ is a point on the dislocation loop L. For some reasons, the relevant literature often reports only the elastic strain and stress fields of dislocations. The elastic lattice rotation field ω_{ml} of dislocations is an equally important quantity in the context of experimental characterization of dislocations in deformed crystals using synchrotron X-ray beams. This field is given by the skew-symmetric part of the displacement gradient, which, for a dislocation loop L, can be written in the form

$$\omega_{ml} = \frac{1}{16\pi}\oint_L dx_k' \left[e_{lik}\left(b_i \frac{\partial}{\partial x_m} + b_m \frac{\partial}{\partial x_i} \right) + e_{imk}\left(b_l \frac{\partial}{\partial x_i} + b_i \frac{\partial}{\partial x_l} \right) \right] \nabla^2 R \tag{3}$$

Deformed crystals typically contain large numbers of dislocations, and the total elastic field associated with the entire ensemble of dislocations is found by summing the contributions due to all individual dislocation loops. In practice, the line integral of the individual loops is converted into a sum of integrals over piecewise linear segments, as currently done in the method of dislocation dynamics [24,25]. In the case of a large dislocation system, the total elastic fields can be split into mean components (or smooth fields) plus fluctuations. That is,

Downloaded 04 Sep 2009 to 160.91.157.167. Redistribution subject to ASME license or copyright; see http://www.asme.org/terms/Terms_Use.cfm

$$\boldsymbol{\varepsilon}(\mathbf{r}) = \bar{\boldsymbol{\varepsilon}}(\mathbf{r}) + \delta\boldsymbol{\varepsilon}(\mathbf{r}), \quad \boldsymbol{\omega}(\mathbf{r}) = \bar{\boldsymbol{\omega}}(\mathbf{r}) + \delta\boldsymbol{\omega}(\mathbf{r}), \quad \boldsymbol{\sigma}(\mathbf{r}) = \bar{\boldsymbol{\sigma}}(\mathbf{r}) + \delta\boldsymbol{\sigma}(\mathbf{r}) \tag{4}$$

with the overbar denoting the mean fields and the delta terms denoting the fluctuations about the mean. The relative importance of the mean field versus fluctuations in the above expressions depends on the spatial resolution of interest. For example, at the macroscale, the mean fields are taken to represent the average quantities over large spatial windows, where the fluctuations are often unimportant. At the mesoscale, however, the mean fields are average quantities over spatial windows on the order of the wavelength of spatial variation of the dislocation density in the crystal. In this case, the fluctuations are important, but their quantification depends on how the mean field itself is defined. When the spatial resolution is extremely small, lower than the distance between individual dislocations, the representation of fields using mean field and fluctuations is no longer applicable, and the fields are interpreted in an exact sense. The characteristics of these three regimes (macro, meso, and micro) are important to keep in mind in interpreting 3D X-ray microscopy data obtained by the present technique.

For mesoscopic length scales, the discrete nature of the dislocation system in crystals can be suppressed in favor of a continuous representation of the mechanical fields of dislocations. In continuum theory, defects are represented in terms of density fields that depend on the nature of the defects themselves. For example, continuous dislocation distributions are described in terms of a tensor field called the dislocation density tensor (see Refs. [28–30]). The solutions of the mechanical fields for continuously distributed dislocations is known [33–35]; for example, within the bounds of linear elasticity theory, the elastic distortion field β^e_{mn} associated with a continuous distribution of dislocations is expressed in terms of the dislocation density tensor $\alpha_{pl}(\mathbf{r})$ as follows:

$$\beta^e_{mn}(\mathbf{r}) = \int dV' c_{ijkl}\hat{u}_{jn,i}(\mathbf{r}-\mathbf{r}')e_{pmk}\alpha_{pl}(\mathbf{r}') \tag{5}$$

The symmetric and skew-symmetric parts of β^e_{mn} are the elastic strain and rotation tensor fields associated with the continuous dislocation distribution. The dislocation density tensor, on the other hand, is defined by the curl of the plastic distortion tensor β^p_{kl},

$$\alpha_{pl} = -e_{pmk}\beta^p_{kl,m} \tag{6}$$

Hooke's law then provides the internal stress distribution from the elastic strain field. In the case of infinitesimal deformation, the elastic rotation tensor has three independent components that define an equivalent axial vector, the components of which are the infinitesimal rotation angles about the x, y, and z (or x_1, x_2, and x_3) axes. The relationship between the rotation tensor and its axial vector is $\omega_{ij}=-e_{ijk}\theta_k$ and $\theta_i=-e_{ijk}\omega_{jk}/2$.

The above equations show that, within the bounds of linear elasticity theory of defects, there is a unique defect (dislocation) field defined for each incompatible plastic distortion, and this defect field completely determines the internal elastic fields in the crystal (elastic strain, elastic lattice rotation, and stress field) [30,33]. The relationships between the defect content (dislocations in the present case, whether discrete or continuous) and the induced elastic fields are given by Eqs. (1)–(3). It is these fields that are measured by the 3D X-ray microscopy technique described here, and the dislocation content is recovered from the differential forms relating dislocation density tensor with the elastic strain field and lattice rotation. This relationship has the form [5,30]:

$$\alpha_{ij} = \kappa_{ji} - \delta_{ij}\kappa_{kk} - e_{ikl}\partial_k\varepsilon_{lj} \tag{7}$$

in which the curvature tensor κ_{ij} is given by the gradient of the lattice orientation vector ω_i,

$$\kappa_{ij} = \theta_{i,j} \tag{8}$$

For cases in which the elastic strains and their gradients are small compared to the curvature, such as might be the case for lightly deformed ductile metals, for instance, Eq. (7) reduces to

$$\alpha_{ij} \approx \kappa_{ji} - \delta_{ij}\kappa_{kk} \tag{9}$$

The above equations are all applicable in the case of infinitesimal deformations. Reference [5] contains the corresponding definitions of the dislocation density tensor in terms of the deformation fields for the case of finite deformation. We note here that the process of plastic deformation of metals leaves behind the following permanent changes in the material: (1) sample shape distortion, which can be seen by slip bands at the specimen surface, (2) internal elastic strain arising due to the dislocation distributions in the crystal, (3) the dislocations themselves, and (4) crystal lattice rotations generated by the distributions of unpaired dislocations (GNDs). While slip traces on surfaces can be characterized quantitatively using techniques such as atomic force microscopy, nondestructive 3D techniques are required for the rest of these signatures of the deformation process; this underscores the importance of 3D X-ray microscopy technique described here in the fundamental investigation of deformation and defects in materials.

4 Dislocation Density Tensor Measurements Using 3D X-Ray Microscopy

The 3D measurement capability discussed in Sec. 2 makes it possible to obtain detailed microstructural information nondestructively on mesoscopic length scales (tenths to hundreds of microns) for deformed as well as nondeformed polycrystalline and single crystal materials. Expressing deformation measurements in terms of dislocation density tensors, $\boldsymbol{\alpha}$ requires a spatially resolved determination of the local lattice curvature $\boldsymbol{\kappa}$ and the curl of the strain tensor, $\nabla\times\boldsymbol{\varepsilon}$, as indicated in Eq. (7); experimental determinations of the curvature and $\nabla\times\boldsymbol{\varepsilon}$ are generated by a numerical differentiation of the spatially resolved orientation and strain measurement data. It is important to keep in mind that the spatial resolution of the X-ray measurements determines the length scale over which dislocations with positive and negative signs are combined to obtain the density of GNDs. That is, only the net rotation can be determined from lattice orientation measurements performed at two points in a sample; information on orientation and strain variations between the two measuring points is not available unless further measurements can be performed between the two points [5,6,19,21,35,36]. Accordingly, the spatial resolution of the experimental technique and the measurement step size determine the length scale of dislocation density fluctuations that can be observed. When the resolution of both the measurements and the calculations is taken into account, direct comparisons of deformation measurements with predictions of theory and modeling [35,36] can be made on an absolute basis. This is a powerful result that will be the subject of ongoing development for both fundamental and applied deformation investigations.

As indicated in Eq. (7), elastic strain as well as lattice curvature is important in determining the dislocation density tensor. Unfortunately, as was mentioned at the end of Sec. 2, spatially resolved measurement of elastic strains in deformed crystals is not always straightforward because of the difficulty of determining deviatoric strain tensors in samples with distorted or streaked Laue diffraction spots. Even in favorable cases (e.g., low deformation, stiff materials) in which the deviatoric strain tensors can be obtained directly from white-beam Laue diffraction measurements, the extraction of full strain tensors (i.e., deviatoric+dilatation strain) requires the specification of at least one absolute lattice parameter [23]. This entails the use of a scanning monochromatic beam [4,13,23]. However, for the special case of "elastic" cylindrical bending of thin Si plates, where anticlastic bending has been demonstrated to vanish at the center of the plate [4,13], it is possible to invoke this constraint to specify zero lattice parameter change along the cylindrical bend axis; this makes it possible to determine the full strain tensor from spatially resolved white-beam measure-

Downloaded 04 Sep 2009 to 160.91.157.167. Redistribution subject to ASME license or copyright; see http://www.asme.org/terms/Terms_Use.cfm

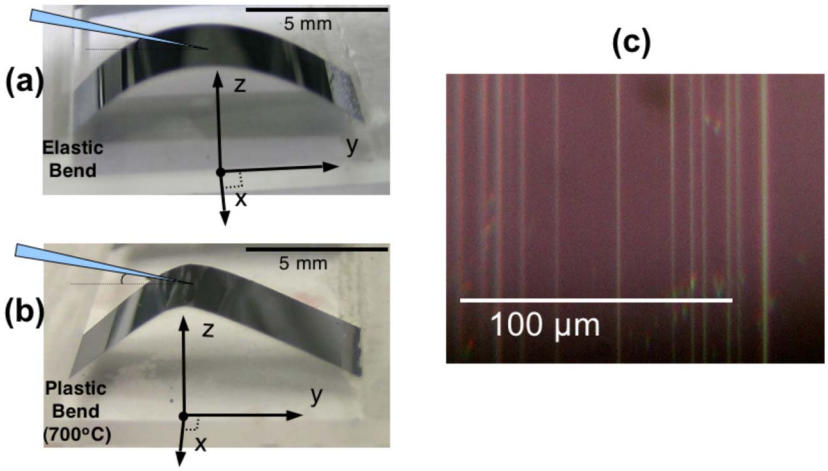

Fig. 3 Optical photographs of cylindrically bent single crystal Si plates indicating the surface-normal direction *z*, surface bend tangent direction *y*, and cylindrical bend axis *x*. (*a*) 42 μm thick Si plate bent elastically into the form of an arch; (*b*) 25 μm thick plastically bent Si plate after annealing to 700°C while in an elastically bent state, where the schematic drawing illustrates that the microbeam enters the sample at a 45 deg angle to the surface at or near the apex of the arch; and (*c*) optical image showing typical slip trace patterns present on the surface of the plastically bent Si plate.

ments alone [4,5]. This constraint will be invoked for dislocation density tensor determinations for the elastically bent Si case to be presented below as well.

There is another important special case for which it is possible to determine dislocation density tensors in plastically deformed materials without explicitly measuring an absolute lattice parameter for each voxel. This is when elastic strains are small so that their gradients are much smaller than the lattice curvature associated with plastic deformation-induced misorientations. This condition can be expected to hold for light deformation in soft, ductile materials, for instance. For such cases, Eq. (9) indicates that measurements of the lattice curvature alone provide a direct measure of the dislocation density tensors $\boldsymbol{\alpha}$. This condition will be shown to apply for the Si plate that was plastically deformed by annealing at 700°C under elastic bending stress.

5 Experiment

Utilizing the procedures described above, 3D X-ray microscopy measurements of the local orientation, strain, and GND density were performed on two deformed (single crystal) Si thin plates. One plate was bent elastically at room temperature and thus, by definition, contained no dislocations; conversely, dislocations were deliberately introduced into the second Si plate by annealing it (under the bending stress) above the brittle-to-ductile temperature. The measurements were performed using white-microbeam Laue diffraction on the XOR/UNI Sector 34 microbeam station at the Advanced Photon Source (APS) [10,16].

The elastically bent sample was 2 mm wide and ~42 μm thick and was bent elastically into the form of an arch and held within a slot in a quartz plate for measurement, as shown in Fig. 3(*a*). This resulted in an (elastically stressed) cylindrical shape with a ~5 mm bend radius at the apex [4,5]; the measurements on this sample were performed at the center of the 2 mm width at the apex of the arch.

The second sample was a 3 mm wide, ~25 μm thick, cylindrically bent Si plate that was heated to 700°C (i.e., above the ~625°C brittle-to-ductile transition temperature for silicon) in the bent condition, held for 30 min in order for plastic deformation to relieve the elastic stress, and slow cooled to room temperature over several hours. The presence of plastic deformation in the annealed sample (shown in Fig. 3(*b*)) is immediately obvious by the sharper, nonconical curvature at the apex of the annealed arch. Further evidence of relief of the elastic bending strain by plastic deformation is provided by the presence of surface slip traces spaced 5–20 μm apart along the [110] direction parallel to the cylindrical bend axis, as shown in Fig. 3(*c*); no slip lines were present at room temperature in the elastically bent state before annealing.

We comment that the samples used in this study are the same as those used in a previous study [5]. The measurements in the previous study demonstrated the capability of measuring dislocation density tensors with spatial resolution along a single line, that is, a line along the microbeam direction, which was perpendicular to the bend axis (i.e., perpendicular to the x axis in the (y,z) plane in Fig. 3). In that study, the gradients of the local orientations and elastic strains (required to obtain the curvature and strain gradients in Eqs. (7) and (9)) for a single line were determined by performing measurements along two additional lines, one after translating the sample 1 μm normal to the beam in the x direction and the other after translating the sample 1 μm normal to the beam in the (y,z) plane.

In the present investigation, we report the first nondestructive measurements of full dislocation density tensors with micron spatial resolution over an areal slice in the interior of a sample. To obtain 3D measurements of dislocation density tensors over a 2D slice, a series of line measurements were made with micron spacing in the (y,z) plane, perpendicular to the cylindrical bend axis (see Fig. 3); further, an identical set of measurements was performed in the (y,z) plane after a 1 μm translation of the sample in the x direction. By making micron spaced in-plane measurements on two parallel planes (i.e., planes separated by 1 μm), it is possible to determine not only the local orientations and elastic strains for each of the x, y, and z components within the two planes, but, by numerical differentiation of the data, also the gradients of each of these quantities. Measurements were made of both the local orientations and elastic strains for the elastically bent sample. The elastic strain tensors were not measured on the plastically deformed sample because of the streaked/distorted nature of the Laue spots (as discussed in Sec. 2 above) and because

Downloaded 04 Sep 2009 to 160.91.157.167. Redistribution subject to ASME license or copyright; see http://www.asme.org/terms/Terms_Use.cfm

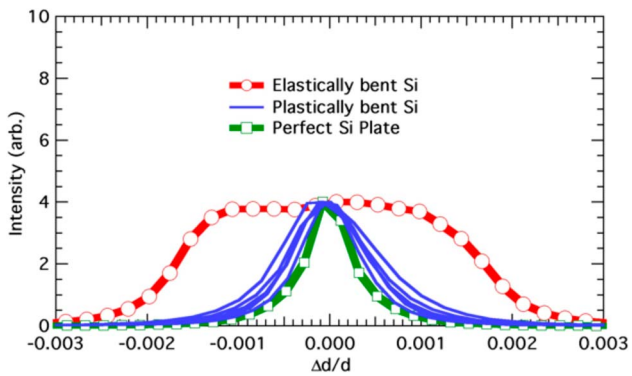

Fig. 4 Energy-scanning monochromatic microbeam measurements of surface-normal lattice strains in the elastically bent (thick line, open circles) and plastically bent (thin lines) Si samples and on a flat, undeformed Si plate (thick line, open squares) as a strain-free reference. The measurements were made at the apex of the elastically bent sample. The measurements on the plastically deformed sample were made near its apex at five separate positions across the sample width, chosen to represent a range of Laue spot streaking. Each of the plastically bent sample strain measurements show some broadening compared to that for the perfect, flat sample; however, all of the plastically deformed sample strain widths are much narrower than that for the elastically bent sample.

measurements discussed immediately below showed that the elastic bending strains were largely relieved during the 700°C anneal.

Figure 4 shows elastic strain measurements (integrated along the microbeam) for both the elastically and plastically deformed Si samples and for a perfect Si wafer as a reference. In these measurements, Bragg scattering from the samples was collected on the CCD area detector as the energy of the microbeam was step scanned through the energy width of the diffraction patterns for either (006) surface-normal or (119) near-normal Bragg reflections. Since each pixel of the CCD constitutes a separate detector, this energy-scanning/CCD-detector technique for determining strain widths is equivalent (in energy space) to standard X-ray line profile measurements of strain gradients in the sample-rotation mode of crystal strain analysis [37]. Although the convergent nature of focused X-ray microbeams leads to a rather broad strain peak width of $\sim 7\times 10^{-4}$ for the case of the perfect Si sample (open squares), the surface-normal strain width in the elastically bent sample is $\sim 3\times 10^{-3}$ (open circles) and the uncertainty in the peak centroid is $\sim 1.5\times 10^{-4}$. The thin lines represent measurements made at a number of representative positions along the apex of the plastically deformed sample; they indicate that (compared to the preanneal strains) the elastic strains were largely relieved by the introduction of dislocations during the 700°C anneal.

Considering that the lattice curvature near the apex of the plastically deformed sample is significantly larger than that in the elastically bent sample (note the rotation full scales in the captions for Figs. 5(*a*) and 6(*a*)), even if elastic strains in the plastically deformed sample approached those in the elastically bent sample, they would not impact $\boldsymbol{\alpha}$ significantly. Therefore, neglecting elastic strains and using Eq. (9) to determine $\boldsymbol{\alpha}$ can be justified for the plastically deformed Si sample. We comment that we believe that the results in Fig. 4 indicate that neglecting elastic strains in determining $\boldsymbol{\alpha}$ for this plastically deformed sample is more reliable than smoothing large-uncertainty white-beam measurements of deviatoric elastic strain, as was done in the previous single-line study [5].

6 Results

Figure 5 shows spatially resolved 3D X-ray microscopy measurements made on the elastically bent sample (see Fig. 3(*a*)), where the top and bottom surfaces of the Si plate define the vertical height of the plots in Fig. 5. Since the X-ray microbeam penetrates the bent Si plates at a 45 deg angle with respect to both the y (horizontal) and z (vertical) axes in the sample (see Figs. 1 and 3), a characteristic parallelogram shaped area normal to the bend axis (i.e., x axis) is defined as successive depth profile measurements are made. The sample is stepped along the y (horizontal) direction after individual depth scans. The top panel (Fig. 5(*a*)) is a color-coded mapping of the local rotations in the sample, and the middle panel (Fig. 5(*b*)) contains spatially resolved measurements of the elastic strain tensors generated by the bending in Fig. 5(*a*). Figure 5(*c*) is a color-coded, spatially resolved plot of the components of the dislocation density tensors $\boldsymbol{\alpha}$ based on Eq. (7), where the gradients of the orientations and elastic strain components were determined by numerical differentiation of the measured data in Figs. 5(*a*) and 5(*b*), respectively.

Considering these data in more detail, the three panels in Fig. 5(*a*) show the x, y, and z components of the rotation vector $\boldsymbol{\theta}=(\theta_x,\theta_y,\theta_z)$ relative to the reference orientation chosen (arbitrarily) as the orientation at the position of the "+" in the figure. We note first of all that only rotations about the x axis (θ_x) are large and that the orientations change uniformly along the y (horizontal) direction as a result of the cylindrical elastic bending around the x axis. The other rotational components in Fig. 5, θ_y and θ_z, are very small in comparison. We note that since the total variation in angle from the upper left corner of the measured area to the lower right position in Fig. 5(*a*) is only about 10 mrad, the orientations and gradients can be expected to have nonnegligible micron-by-micron fluctuations even with the higher angular resolution ~0.01 deg (~0.2 mrad) measurement capability of the 3D X-ray microscopy method.

Figure 5(*b*) shows a color-coded plot of the components of the (full) elastic strain tensor ε_{ij} as a function of position within the slice. ε_{ij} is given in terms of the deviatoric strain ε'_{ij} and the dilatational strain Δ by $\varepsilon_{ij}=\varepsilon'_{ij}+\Delta/3\delta_{ij}$, where Δ was obtained from depth-resolved white-beam measurements of ε'_{ij} and by using the additional fact that anticlastic bending vanishes except very near the edge of the sample [4,13] for cylindrically bent thin Si plates. In particular, as shown by direct measurements of anticlastic bending in bent Si plates [13] and as discussed previously [4,5,13], the condition of vanishing anticlastic bending condition implies that $\varepsilon_{xx}=0$ at all positions except near the edge of the plate. Therefore, $\varepsilon'_{xx}=-\Delta/3$ provides a point-by-point measure of the local dilatation strain $\Delta/3$, where Δ is the trace of ε_{ij}. The y component of the strain, ε_{yy}, is positive at the top of the arch (i.e., along the bend) due to stretching, and compressive (negative) at the bottom. In addition to ε_{yy}, we note that the only component with measurable strain under cylindrical bending in Si is ε_{zz}, which represents Poisson contraction normal to the Si surface at the top of the plate and Poisson expansion at the bottom.

Using Eq. (7), the CND density tensor $\boldsymbol{\alpha}$ for the 1 μm spatial steps of these measurements is given by the nine components in Fig. 4(*c*). Except for the occurrence of isolated fluctuations (generated by the ~0.01 deg angular orientation measurement uncertainties and $\sim 1-2\times 10^{-4}$ strain component uncertainties) at points distributed throughout the data, the lattice curvature is fully accounted for by the elastic strain gradients. Thus, the measurements show the known result that the GND density is zero for elastically bent Si plates.

Although this represents a trivial case in one sense and is, of course, an extension of previous measurements performed along single lines [5,13], it is the first direct demonstration of this result with micron spatial resolution over a mesoscopic areal slice within a 3D sample. As such, it demonstrates the principle of the technique for measuring the GND density using a sample with a known result (i.e., elastic bending without dislocations), and it provides a visual illustration of the information contained in the individual components of the tensors. Moreover, the nonzero fluc-

Downloaded 04 Sep 2009 to 160.91.157.167. Redistribution subject to ASME license or copyright; see http://www.asme.org/terms/Terms_Use.cfm

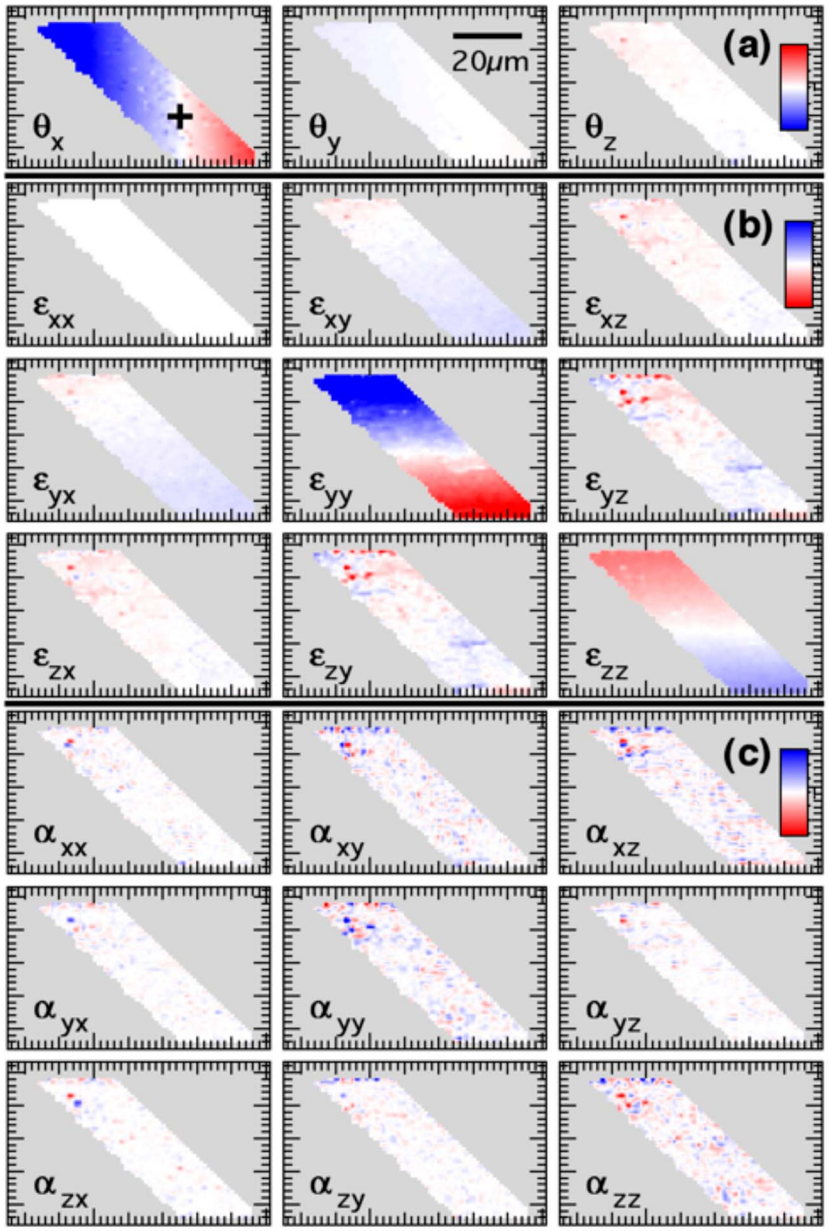

Fig. 5 Color-coded mapping of local orientations, elastic strain tensors, and dislocation density tensors over a vertical slice perpendicular to the bend axis of the elastically bent Si arch in Fig. 3(*a*). (*a*) *x*, *y*, and *z* components of the rotation vector $\theta=(\theta_x,\theta_y,\theta_z)$ relative to the orientation at the "+" in the figure; (*b*) the elastic strain tensor mapping for the elastically bent Si sample; (*c*) GND dislocation density tensor mapping for elastically bent Si, showing no statistically significant GNDs. Full-scale colors correspond to ±5 mrad in (*a*), $\pm 3\times 10^{-3}$ strain in (*b*), and 3 mrad/μm$=0.95\times 10^{9}$ cm^{-2} in (*c*). In addition to the 20 μm length bar at the top that pertains to all graphs in the figure, tick marks with 2 μm spacing are included on each axis to further define the length scale.

tuations in the results provide a measure of the level of uncertainties in the measurements since the Si plates used initially have negligible inhomogeneities.

From the example of elastic bending in a Si plate, we now turn to the measurements on the plastically bent Si sample. In Fig. 6(*a*), we show local lattice orientations for the plastically deformed sample; as in Fig. 5, for the elastically bent sample, the rotational deformation is almost exclusively around the x axis. However, unlike the elastically bent case, the curvature is not at all uniformly distributed along the y (horizontal) direction. Rather, the plastic deformation-induced rotations in Fig. 6(*a*) are highly localized in a region of strong curvature (the light area) of θ_x, where the orientations are changing rapidly from a highly positive to a highly negative orientation (blue to red) near the center of the measured area.

Since we concluded from Fig. 4 that the annealed sample contained only a small amount of residual elastic strain after the anneal, we use Eq. (9) to obtain the dislocation density tensors $\boldsymbol{\alpha}$ directly from the lattice curvature κ_{ji}, the gradients of the local orientations in Fig. 6(*a*). Accordingly, the components of $\boldsymbol{\alpha}$ in Fig.

Downloaded 04 Sep 2009 to 160.91.157.167. Redistribution subject to ASME license or copyright; see http://www.asme.org/terms/Terms_Use.cfm

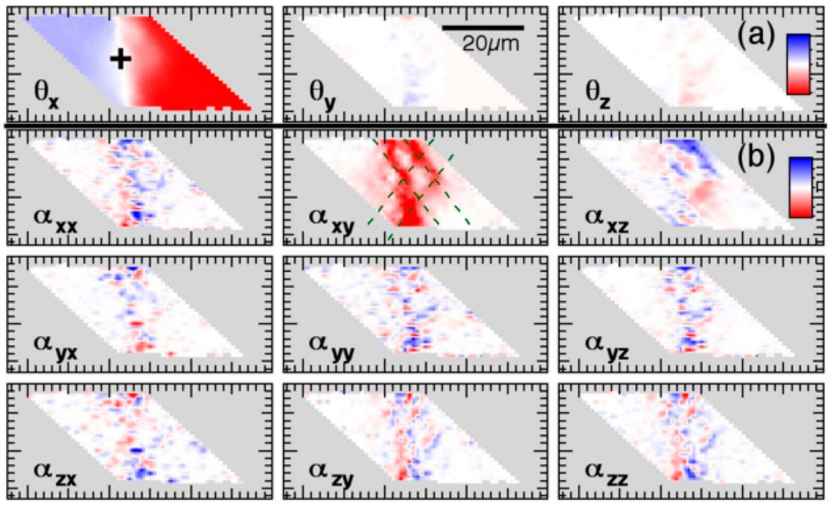

Fig. 6 Color-coded mapping of local rotations and dislocation density tensors on a slice perpendicular to the bend axis of the 700°C annealed plastically deformed Si sample in Fig. 3(*b*). (*a*) *x*, *y*, and *z* components of the rotation vector $\theta = (\theta_x, \theta_y, \theta_z)$ relative to the orientation at the "+" in the figure; (*b*) dislocation density tensor mapping of the plastic deformation-induced GNDs showing α_{xy} to be the dominant component. Full-scale colors correspond to ±20 mrad in (*a*) and 3 mrad/μm$=0.95\times10^9$ cm^{-2} in (*b*). In addition to the 20 μm length bar at the top of the figure that pertains to all graphs, tick marks with 2 μm spacing are included on each axis to further define the length scale.

6(*b*) (obtained using Eq. (9)) provide the spatial distribution of the GND density for the plastically deformed Si sample. The α_{xy} component of the dislocation density tensor clearly contains the dominant GND density although α_{xz} contains significant weight as well. It is, of course, not a surprise that the α_{xy} and α_{xz} components are large since they are derived from the y and z gradients of θ_x, which is by far the largest rotational component. We note that the GND distribution in α_{xy} has a relatively complex microstructure with a few micron length scale. As indicated by the dashed lines in α_{xy} (which denote the angle of {111} slip-plane traces), the strong bands of deformation tend to be aligned along the slip planes, but they do not follow a single slip direction through the entire plate.

7 Discussion

We emphasize first of all that the thrust of this paper is to demonstrate the ability to characterize GND density in terms of the dislocation density tensor $\boldsymbol{\alpha}$ over a 2D slice on mesoscopic length scales using 3D X-ray microscopy measurements. Although comments regarding plastic deformation in Si will be presented, a detailed study of plastic deformation in Si is outside the scope of this paper. These micron-resolution measurements represent the first dislocation density tensor measurements reported over a 2D slice on mesoscopic length scales (tens of microns). The measurements, performed on a plane perpendicular to the bend axis in cylindrically elastically and plastically deformed thin silicon plates, highlight present 3D X-ray microscopy capabilities, and they also indicate some of the limitations of the method. In this section, we discuss the results presented above and provide a perspective on the use of such measurements in relation to computer simulations and multiscale modeling and on the potential role of dislocation density tensors in fundamental investigations of deformation in ductile materials [19–21,38–41].

The results for the elastically bent Si sample in Fig. 5 provide an illustrative test as well as a demonstration of the X-ray microscopy method for determining GND density (or the lack thereof in this completely elastic case) from measurements of the lattice curvature and the elastic strain tensor. The color scale of the figures is in units of radians/micron, in accordance with the units of lattice curvature and elastic strain gradients obtained from the X-ray measurements. The conversion from curvature κ in rad/μm to dislocation density for Burgers vector b is given by $\rho_{\mathrm{GND}}=\kappa/b$; for Si, 1 deg/$\mu$m$\sim5.5\times10^9$/cm^2. Considering the three mrad full-scale color of the plots, this leads to full-scale $\boldsymbol{\alpha}$ values of 0.95×10^9 in Figs. 5(*c*) and 6(*b*). The elastic bend case in Fig. 5 demonstrates directly the (offsetting) balance between elastic strain gradients and lattice curvature in brittle materials, where dislocations are not introduced during bending. On the other hand, Fig. 6 demonstrates a case in which the local orientation gradients in high temperature (700°C) plastically deformed silicon are not associated with elastic strain gradients but rather with the presence of a strong GND density.

As we noted above, the GND density in Fig. 6(*b*) is largest for the α_{xy} component. We note also that the strongly deformed region is inhomogeneous and highly localized within the ~30 μm measurement region. The localized nature of the GND density within the sample is consistent with the ~5–20 μm spacing of surface slip traces in Fig. 3(*c*) and underscores the highly nonuniform nature of deformation for Si under such conditions, due in part to the lack of nucleation sites in perfect crystals. The spatial distribution of the GNDs is significant in that lattice slip seems to be activated preferentially along the traces (dashed lines) of two {111} slip planes. While it is outside the scope of this paper to analyze the details of the dislocation mediated plastic deformation, it is interesting to note the similarity between the dislocation bands in α_{xy} and the discrete dislocation simulation results of Cleveringa et al. [41] for plastic bending of plates. The fact that all of the GND density in the α_{xy} panel is red in color indicates that all of the rotations have the same sign within the 1 μm step size of the measurements. On the other hand, the presence of both blue and red regions in the α_{xz} component indicates the presence of counter-rotations along the z direction; this indicates that the GND density changes sign. The small areas of red and blue GND density in the central portion of the components of $\boldsymbol{\alpha}$ in the second and third rows appear to be associated in general with local regions of sharp changes in α_{xy}. Since these small regions of GND

Downloaded 04 Sep 2009 to 160.91.157.167. Redistribution subject to ASME license or copyright; see http://www.asme.org/terms/Terms_Use.cfm

density result from the gradients of the orientations in Fig. 6(*a*), they suggest the presence of rather complex local rotations; however, measurement uncertainties need to be considered.

Regarding uncertainties, a full statistical analysis has not been performed, but the rms value of the GND density in elastically bent Si (Fig. 5(*c*)) is $\sim 1.5\times 10^8$ cm^{-2}. Since the actual GND density is known to be zero for elastic bending, we take this value as a measure of the present limit on the sensitivity of the 3D X-ray microscopy method for measuring GND density. In the plastically deformed sample, the GND density in the strongly distorted bands in α_{xy} is $\sim 1.3\times 10^9$ cm^{-2}, which is then about a factor of 10 above the $\sim 1.5\times 10^8$ cm^{-2} sensitivity limit. However, for some of the other GND structures distributed throughout the plastically deformed silicon, we cannot distinguish entirely between fluctuations resulting from uncertainties in the measurements and gradients generated by GNDs. If we use the level of fluctuations in Fig. 5(*c*) as a rough measure of the uncertainties, the more dense GND structures that roughly follow the pattern of α_{xy} are likely to reflect local rotations around the y and z axes. We remark that in the data presented here, we have not employed smoothing algorithms, nor have we used hand processing to locate and correct spurious results; therefore, it can be expected that some of the structures are not entirely real. Since hand processing of a large number of voxels included in such plots is neither feasible nor desirable, it will be important to develop robust techniques such as those developed for electron backscattering scanning microscopy (EBSM) for identifying and dealing with erroneous results.

The overall situation regarding the measurement of elastic strains and strain gradients as well as the curvature in highly deformed, ductile materials is worth reiterating because the measurement of full elastic strain tensors is intrinsically difficult when Bragg reflections are distorted or streaked. Fortunately, as evidenced by the monochromatic measurements in Fig. 4, elastic strains and gradients in deformed ductile materials tend to be small compared to the deformation-induced local lattice curvature. Therefore, it will often be possible to determine the dislocation tensors for ductile deformation using the lattice curvature $\boldsymbol{\kappa}$ only, as given by Eq. (9). On the other hand, hard (but not brittle) materials such as deformed Ti–Al alloys are likely to contain significant elastic strains as well as large plastic deformation. Accordingly, the development of robust 3D measurement and analysis techniques for determining the elastic strain tensors in plastically deformed materials with highly distorted diffraction spots is important.

We consider now the implications of the capabilities demonstrated here to measure both the magnitude and spatial distribution of the GND density with micron spatial resolution in three dimensions. With the long-term goal of achieving a predictive understanding of deformation in crystalline materials, it is important that the results of experimental, theoretical, and computational investigations be compared directly. The continuum theory of dislocation fields [20,21,38,39] provides strong insight into the deformation at the macroscale with the aid of constitutive law formulations and finite element modeling (FEM), and discrete dislocation dynamics method implementations [24,25,41] provide a remarkable level of insight into the complex interactions between individual dislocations and groups of dislocations at the microscale. The development of robust theoretical methods such as the statistical theory of dislocations [26,27] to obtain a similar understanding of deformation processes on mesoscopic length scales is critical for continued progress toward a fundamental understanding of dislocation mediated deformation.

Dislocation dynamics deformation simulations produce local rotations and elastic strain fields (the fundamental quantities measured by 3D X-ray microscopy) with significant density fluctuations [24,25]; contrary to continuum formulations, the discreteness of the dislocation system is an intrinsic feature of the method. Therefore, a comparison of experimental measurements with the results of dislocation dynamics requires processing of the elastic strain and rotation fields to extract the smooth component as well as the fluctuation components, as indicated by Eqs. (4). On the other hand, in macroscopic situations, the continuum theory of dislocation fields (with appropriate constitutive assumptions) yields smooth fields over length scales that are long compared with the length scale of dislocation field fluctuations in the discrete dislocation dynamics method [38,39]. Because neither of the limiting cases is able to address the mesoscale appropriately, the statistical theory of dislocations has been formulated to include both smooth fields and fluctuations [31]. Accordingly, it is expected that predictions made by the statistical theory will be better suited for comparison with mesoscale X-ray microbeam measurements and will provide an interpretation of both the mean field behavior and the fluctuations in the GND density. Currently, the continuum theory of dislocation fields is the most highly developed of these techniques for comparison with experiments, and both 2D and 3D results are now available [20,21,38,39,42]. Dislocation dynamics simulations can now be used to simulate the response of materials with uniform (tension or compression) loading for small deformation levels, say, up to $\sim 1\%$. The statistical theory, addressing the mesoscale directly, is not fully solved yet, although applications to simple cases have been tried [38].

In focusing the present demonstration on X-ray microbeam measurements of the dislocation density tensor, we underscore the potential for a direct and absolute comparison between experimental and computational results for deformation in crystalline materials on mesoscopic length scales. As emphasized in Sec. 3 above, simulations and multiscale modeling of local rotation and elastic strain deformation on mesoscopic length scales can be cast in the form of dislocation density tensors, and the spatial resolution of the simulations can be coarse grained to match the spatial resolution of the experimental measurements. It is important to keep in mind that the dislocation density tensor components given by Eqs. (7)–(9), and as measured by X-rays, are direct representations of the nine components of the local lattice curvature and strain gradient tensors. Therefore, a comparison of micron (or submicron)-resolution 3D X-ray microscopy measurements on deformed materials (tension, compression, bending, indents, etc.) with simulations and modeling of dislocation density tensors can indeed provide stringent and quantitative tests of our understanding of deformation processes.

We emphasize that within the length scales and spatial resolution of 3D X-ray microscopy measurements, direct and absolute comparisons of experimentally measured dislocation density tensors can be made not only with top-down FEM crystal plasticity models, strain gradient models, etc., but also with bottom-up computations such as discrete dislocation modeling and the (presently under development) statistical dislocation density models. It is worth noting, however, that since crystalline materials have more than nine slip systems, in general, the dislocation density tensor cannot provide "unique" determinations of the GND density in terms of active slip systems [43]. Face-centered cubic materials have 12 edge-dislocation slip systems and 6 screw systems, for instance. Nevertheless, micron and longer length scale correlations of strong dislocation density banding with particular slip planes, such as in the α_{xy} component in Fig. 6(*b*), are expected to be of significant value in analyzing and understanding deformation distribution results.

With the development that is currently ongoing, synchrotron X-ray microbeam techniques such as submicron-resolution 3D X-ray microscopy [4–10] and high-energy 3D crystal microscopy [9,11,44,45] can be expected to provide increasingly detailed nondestructive information on local lattice rotations and elastic strains over mesosopic length scales ranging from tenths of microns to hundreds of microns. This will generate new opportunities for combined experimental and computational probes of the fundamental aspects of deformation in crystalline materials. Although the measurements reported here were performed with ~ 0.5 μm microbeams and 1 μm step sizes, microbeams in the sub-100-nm

Downloaded 04 Sep 2009 to 160.91.157.167. Redistribution subject to ASME license or copyright; see http://www.asme.org/terms/Terms_Use.cfm

range are now becoming available [46], and obtaining the requisite thermal and vibration stability measurement conditions is under development. Therefore, ~100 nm resolution microstructural measurements using techniques analogous to those discussed here can be expected in the foreseeable future.

8 Summary

We have recalled the basic elements of the 3D X-ray microscopy technique, and we have shown that 3D X-ray microscopy measurements of elastic and plastic deformation in cylindrically bent silicon plates provide a direct measure of the GND density with micron spatial resolution. In particular, the ability to measure (nondestructively) the dislocation density tensor with micron spatial resolution in plastically deformed Si plates was demonstrated for the first time for 2D slices on mesoscopic length scales. The potential to use 3D X-ray microscopy measurements of dislocation density tensors for detailed and absolute comparisons with computer simulations and multiscale modeling has been discussed. Present limitations of the technique have been considered along with the outlook in the future for sub-100-nm-spatial resolution measurements.

Acknowledgment

Research sponsored by the Department of Energy, Office of Science, Division of Materials Sciences and Engineering. Measurements were performed on the XOR/UNI Sector 34 ID beamline at the APS. One of the authors (W.L.) and the operation of the APS were sponsored by the Department of Energy, Division of Scientific User Facilities.

References

[1] Hirth, J. P., and Lothe, J., 1982, *Theory of Dislocations*, Wiley, New York.
[2] Nabarro, F. R. N., 1987, *Theory of Crystal Dislocations*, Dover, New York.
[3] Jourdan, C., and Gastaldi, J., 1977, "X-Ray Topographic Investigation of Dislocations in Ti Single Crystals Grown by Recrystallization," Phys. Status Solidi A, **43**, pp. 425–435.
[4] Larson, B. C., Yang, W., Ice, G. E., Budai, J. D., and Tischler, J. Z., 2002, "Three-Dimensional X-Ray Structural Microscopy With Submicrometre Resolution," Nature (London), **415**, pp. 887–890.
[5] Larson, B. C., El-Azab, A., Yang, W., Tischler, J. Z., Liu, W., and Ice, G. E., 2007, "Experimental Characterization of the Mesoscale Dislocation Density Tensor," Philos. Mag., **87**, pp. 1327–1347.
[6] Yang, W., Larson, B. C., Tischler, J. Z., Ice, G. E., Budai, J. D., and Liu, W., 2004, "Differential-Aperture X-Ray Structural Microscopy: A Submicron-Resolution Three-Dimensional Probe of Local Microstructure and Strain," Micron, **35**, pp. 431–439.
[7] Yang, W., Larson, B. C., Pharr, G. M., Ice, G. E., Budai, J. D., Tischler, J. Z., and Liu, W. J., 2004, "Deformation Microstructure Under Microindents in Single-Crystal Cu Using Three-Dimensional X-Ray Structural Microscopy," J. Mater. Res., **19**, pp. 66–72.
[8] Levine, L. E., Larson, B. C., Yang, W., Kassner, M. E., Tischler, J. Z., Delos-Reyes, M. A., Fields, R. J., and Liu, W., 2006, "X-Ray Microbeam Measurements of Individual Dislocation Cell Elastic Strains in Deformed Single-Crystal Copper," Nat. Mater., **5**, pp. 619–622.
[9] Larson, B. C., and Lengeler, B., 2004, "High Resolution Three-Dimensional X-Ray Microscopy," MRS Bull., **29**, pp. 152–156.
[10] Ice, G. E., and Larson, B. C., 2004, "Three-Dimensional X-Ray Structural Microscopy Using Polychromatic Microbeams," MRS Bull., **29**, pp. 170–176.
[11] Poulsen, H. F., Jensen, D. J., and Vaughan, G. B. M., 2004, "Three-Dimensional X-Ray Diffraction Microscopy Using High-Energy X-Rays," MRS Bull., **29**, pp. 166–169.
[12] Poulsen, H. F., 2004, *Three-Dimensional X-Ray Diffraction Microscopy: Mapping Polycrystals and Their Dynamics* (Springer, Berlin, 2004).
[13] Yang, W., Larson, B. C., Ice, G. E., Tischler, J. Z., Budai, J. D., Chung, K.-S., and Lowe, W. P., 2003, "Spatially Resolved Poisson Strain and Anticlastic Curvature Measurements in Si Under Large Deflection Bending.," Appl. Phys. Lett., **82**, pp. 3856–3858.
[14] Poulsen, H. F., Lienert, U., and Pantleon, W., 2005, "Characterisation of Orientation Distributions of Individual Grains Within Deformed Metals," Mat. Sci. Technol., **21**, pp. 1397–1400.
[15] Margulies, L., Winther, G., and Poulsen, H. F., 2001, "In Situ Measurement of Grain Rotation During Deformation of Polycrystals," Science, **292**, pp. 2392–2394.
[16] Ice, G. E., Larson, B. C., Yang, W., Budai, J. D., Tischler, J. Z., Pang, J. W. L., Barabash, R. I., and Liu, W., 2005, "Polychromatic X-Ray Microdiffraction Studies of Mesoscale Structure and Dynamics," J. Synchrotron Radiat., **12**, pp. 155–162.
[17] Nye, J. F., 1953, "Some Geometric Relations in Dislocated Crystals," Acta Metall., **1**, pp. 153–162.
[18] El-Azab, A., 2000, "The Boundary Problem of Dislocation Dynamics," Modell. Simul. Mater. Sci. Eng., **8**, pp. 37–54.
[19] El-Azab, A., 2000, "Statistical Mechanics Treatment of the Evolution of Dislocation Distributions in Single Crystals," Phys. Rev. B, **61**, pp. 11956–11966.
[20] Limkumnerd, S., and Sethna, J. P., 2006, "Mesoscale Theory of Grains and Cells: Crystal Plasticity," Phys. Rev. Lett., **96**, p. 095503.
[21] Limkumnerd, S., and Sethna, J. P., 2007, "Stress-Free States of Continuum Dislocation Fields: Rotations, Grain Boundaries, and the Nye Dislocation Density Tensor," Phys. Rev. B, **75**, p. 224121.
[22] Larson, B. C., Yang, W., Tischler, J. Z., Ice, G. E., Budai, J. D., Liu, W., and Weiland, H., 2004, "Micron-Resolution 3-D Measurement of Local Orientations Near a Grain-Boundary in Plane-Strained Aluminum Using X-Ray Microbeams," Int. J. Plast., **20**, pp. 543–560.
[23] Chung, J. S., and Ice, G. E., 1999, "Automated Indexing for Texture and Strain Measurement With Broad-Bandpass X-Ray Microbeams," J. Appl. Phys., **86**, pp. 5249–5255.
[24] Weygand, D., Friedman, L. H., Van der Giessen, E., and Needleman, A., 2002, "Aspects of Boundary-Value Problem Solutions With Three-dimensional Dislocation Dynamics," Modell. Simul. Mater. Sci. Eng., **10**, pp. 437–468.
[25] Weygand, D., and Gumbsch, P., 2005, "Study of Dislocation Reactions and Rearrangements Under Different Loading Conditions," Mater. Sci. Eng., A, **400–401**, pp. 158–161.
[26] El-Azab, A., Deng, J., and Tang, M., 2007, "Statistical Characterization of Dislocation Ensembles," Philos. Mag., **87**, pp. 1201–1223.
[27] El-Azab, A., 2006, "Statistical Mechanics of Dislocation Systems," Scr. Mater., **54**, pp. 723–727.
[28] Kosevich, A. M., 1979, "Crystal Dislocations and the Theory of Elasticity," *Dislocations in Solids*, F. R. N. Nabarro, ed., North-Holland, Amsterdam, Vol. 1, pp. 33–141.
[29] Mura, T., 1968, "Continuum Theory of Dislocations and Plasticity," *Mechanics of Generalized Continua*, E. Kröner, ed., Springer-Verlag, New York, pp. 269–278.
[30] Kröner, E., 1981, "Continuum Theory of Defects," *Physics of Defects*, R. Balian, M. Kléman, and J.-P. Poirier, eds., North-Holland, Amsterdam, pp. 217–315.
[31] El-Azab, A., Zaiser, M., and Busso, E., 2007, "Density-Based Modelling of Dislocations," Philos. Mag., **87**(8–9), pp. 1159–1160.
[32] Eshelby, J. D., 1956, "The Continuum Theory of Lattice Defects," Solid State Phys., F. Seitz and D. Turnbull, eds., volume **3**, pp. 79–144.
[33] Mura, T., 1987, *Micromechanics of Defects in Solids*, 2nd ed., Martinus Nijhoff, Dordrecht, The Netherlands.
[34] Kossecka, E., 1974, "Mathematical Theory of Defects. Part I. Statics," Arch. Mech., **26**, pp. 995–1010.
[35] Gurtin, M. E., 2002, "A Gradient Theory of Single-Crystal Viscoplasticity That Accounts for Geometrically Necessary Dislocations," J. Mech. Phys. Solids, **50**, pp. 5–32.
[36] Needlemann, A., and Sevillano, J. G., 2003, "Preface to the Viewpoint Set on: Geometrically Necessary Dislocations and Size Dependent Plasticity," Scr. Mater., **48**, pp. 109–111.
[37] Ungar, T., Mughrabi, H., Rönnpagel, D., and Wilkens, M., 1984, "X-Ray Line-Broadening Study of the Dislocation Cell Structure in Deformed (001)-Oriented Vopper Single Crystals," Acta Metall., **32**, pp. 333–342.
[38] Acharya, A., and Roy, A., 2006, "Size Effects and Idealized Dislocation Microstructure at Small Scales: Predictions of a Phenomenological Model of Mesoscopic Field Dislocation Mechanics: Part I," J. Mech. Phys. Solids, **54**, pp. 1687–1710.
[39] Roy, A., and Acharya, A., 2006, "Size Effects and Idealized Dislocation Microstructure at Small Scales: Predictions of a Phenomenological Model of Mesoscopic Field Dislocation Mechanics: Part II," J. Mech. Phys. Solids, **54**, pp. 1711–1743.
[40] Zaiser, M., Nikitas, N., Hochrainer, T., and Aifantis, E. C., 2007, "Modelling Size Effects Using 3D Density-Based Dislocation Dynamics," Philos. Mag., **87**, pp. 1283–1306.
[41] Cleveringa, H. H. M., Van der Giessen, E., and Needleman, A., 1999, "A Discrete Dislocation Analysis of Bending," Int. J. Plast., **15**, pp. 837–868.
[42] Ma, A., Roters, F., and Raabe, D., 2006, "A Dislocation Density Based Constitutive Model for Crystal Plasticity FEM Including Geometrically Necessary Dislocations," Acta Mater., **54**, pp. 2169–2179.
[43] Arsenlis, A., and Parks, D. M., 1999, "Crystallographic Aspects of Geometrically-Necessary and Statistically-Stored Dislocation Density," Acta Mater., **47**, pp. 1597–1611.
[44] Jakobsen, B., Poulsen, H. F., Lienert, U., and Pantleon, W., 2007, "Direct Determination of Elastic Strains and Dislocation Densities in Individual Subgrains in Deformation Structures," Acta Mater., **55**, pp. 3421–3430.
[45] Wert, J. A., Huang, X., Winther, G., Pantleon, W., and Poulsen, H. F., 2007, "Revealing Deformation Microstructures," Mater. Today, **10**, pp. 24–32.
[46] Liu, W., Ice, G. E., Tischler, J. Z., Khounsary, A., Liu, C., Assoufid, L., and Macrander, A. T., 2005, "Short Focal Length Kirkpatrick-Baez Mirrors for a Hard X-Ray Nanoprobe," Rev. Sci. Instrum., **76**, pp. 113701–113706.

Downloaded 04 Sep 2009 to 160.91.157.167. Redistribution subject to ASME license or copyright; see http://www.asme.org/terms/Terms_Use.cfm